OPEN ACCESS
JOURNAL OF ADVANCED DIELECTRICS
Vol. 11, No. 3 (2021) 2140006 (6 pages)

DOI: 10.1142/S2010135X21400063

Structural, microstructural and dielectric characterizations of $(Bi_{0.5}Na_{0.5})TiO_3$ based lead-free ferroelectric ceramics

B. R. Moya*,†, A. C. Silva*, A. Peláiz-Barranco‡ and J. D. S. Guerra*,§

*Grupo de Ferroelétricos e Materiais Multifuncionais
Instituto de Física, Universidade Federal de Uberlândia
Uberlândia, Minas Gerais 38408-100, Brazil

†Departamento de Física e Química, UNESP
Campus de Ilha Solteira, São Paulo 15385-000, Brazil

‡Grupo de Materiales Ferroicos
Facultad de Física-Instituto de Ciencia y Tecnología de Materiales
Universidad de La Habana, La Habana 10400, Cuba

§santos@ufu.br

Received 5 February 2021; Revised 30 April 2021; Accepted 19 May 2021; Published 23 June 2021

$(1–x)Bi_{0.5}Na_{0.5}TiO_3–xBaTiO_3$ lead-free ceramics have been obtained from the conventional solid-state reaction sintering method. The structural properties were investigated from X-ray diffraction and Raman spectroscopy techniques. Results revealed well-crystallized ceramic samples with perovskite structure. Microstructural properties, obtained from scanning electron microscopy measurements, have shown high density with very low porosity level. The dielectric response, analyzed as a function of the temperature and several frequencies, showed very broad peaks with a strong frequency dependence of the temperature for the maximum dielectric permittivity for the modified system. Results were analyzed considering the influence of the $BaTiO_3$ content on the studied physical properties.

Keywords: Lead-free; BNT; Raman spectroscopy; dielectric response.

1. Introduction

Ferroelectric (FE) materials have been of great importance over the last several decades because of their excellent physical properties,[1] thus making them promising for potential technological applications.[2] For specific compositions, however, additional interesting properties, which have been related to the appearance of the antiferroelectric (AFE) phase, stand out, thus enhancing their applicability spectrum including their integration in energy storage devices as well as electrocaloric refrigerators.[3,4]

Therefore, intense efforts have been dedicated by the scientific community during the last years for the development of lead-free ferroelectrics with enhanced piezoelectric properties[5] because of environmental concerns,[6] thus replacing the lead-based compounds.[7,8] Among the extensive number of lead-free systems that have been reported in the literature, the $(Bi_{0.5}Na_{0.5})TiO_3$ (BNT), $(Bi_{0.5}K_{0.5})TiO_3$ (BKT) and $(K_{0.5}Na_{0.5})NbO_3$ (KNN) systems have received special attention because of their excellent piezoelectric response,[9–11] showing piezoelectric coefficient (d_{33}) values around 64, 69 and 80 pC/N, respectively.[10,12,13] However, in comparison with those pure BNT, BKT and KNN compounds, the piezoelectric properties have shown to be enhanced for $(1–x)Bi_{0.5}Na_{0.5}TiO_3–xBaTiO_3$ (BNT–BT) solid-solution revealing remarkable d_{33} values (~120–180 pC/N) at room temperature.[14–16] For instance, the BNT–BT system has revealed as a promising lead-free piezoelectric system, because of the existence of a morphotropic phase boundary (MPB) where the rhombohedral (R3*c*) and tetragonal (P4*mm*) phases coexists.[17,18] Is, therefore, for compositions around the MPB that the BNT–*x*BT system shows enhanced physical properties,[19] such as high electromechanical coefficient,[20] thus leading to an excellent piezoelectric performance, improved dielectric response[14,15,21] and remarkably low coercive field.[15] Such improvements have been ascribed to the polarization rotation due to the coexistence between the involved phases.

In the current literature, there have been reported up today two phases' diagrams for the BNT–BT ceramic system, which in fact reveal very different characteristics. According to Takenaka *et al.*,[17] the rhombohedral (R3*c*) and tetragonal (P4*mm*) ferroelectric (FE) phases and the tetragonal (P4*bm*) AFE phase coexist in the BNT–BT system with a remarkable temperature dependence, while a sudden transition from rhombohedral (R3*c*) to tetragonal (P4*mm*) FE phase is

§Corresponding author.

observed for compositions around 6 at.% BT, characterizing a clear MPB. However, a different behavior around the MPB has been reported by Ma and Tan[18] for the same BNT–BT compositions, where a very broad region owing to the AFE phase is observed, which extends over a very wide BT compositional range from around 6 up to 10 at.%. In this case, a new concept of AFE "relaxor" has been proposed for describing the single short-range AFE order for this phase. The results suggest that phase transitions induced by an external electric field should be taken into account in the optimization of the piezoelectric properties in these lead-free ceramics. Therefore, detailed investigations are needed in order to better elucidate a real phase diagram for this system.

The aim of the present work is to investigate the physical properties of $(Bi_{0.5}Na_{0.5})_{1-x}Ba_xTiO_3$ (BNT–BT) lead-free ceramics, where $x = 0$ and 5 at.%, obtained from the solid-state reaction sintering method. In particular, the structural properties have been analyzed from X-ray diffraction (XRD) and Raman spectroscopy techniques. On the other hand, scanning electronic microscopy (SEM) allowed the study of the microstructural characteristics of the studied samples and the dielectric response has been investigated from the temperature dependence of the complex dielectric permittivity. The influence of the barium doping on the studied properties has been taken into account.

2. Experimental Procedure

$(1–x)Bi_{0.5}Na_{0.5}TiO_3–xBaTiO_3$ ($x = 0$ and 5 at.%) ceramic samples, named as BNT and BNT–5BT for 0 and 5 at.%, respectively, were prepared by the conventional solid-state reaction sintering method.[22] High-purity analytical-grade precursors were used as starting reagents. Figure 1 summarizes the steps followed for the sintering process of the ceramics.

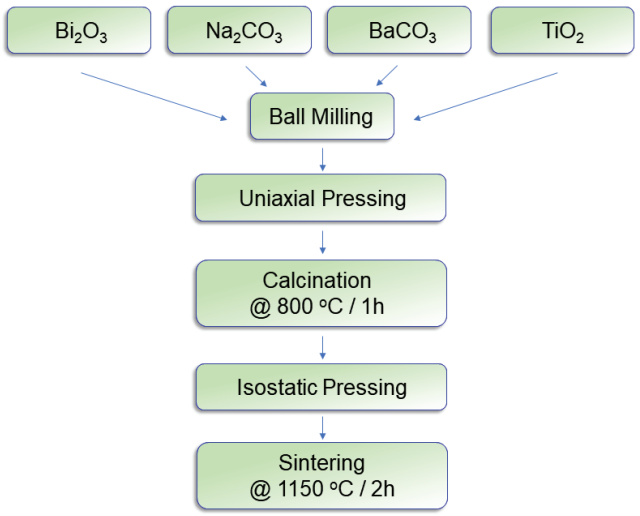

Fig. 1. Schematic diagram for the synthesis of the studied BNT and BNT–BT ceramics.

The structural properties were investigated, at room temperature, from both the XRD technique and Raman spectroscopy. The XRD data was collected on powdered ceramic samples using a Shimadzu XRD-6000 diffractometer with $CuK\alpha_1$ radiation ($\lambda = 1.54056$ Å). The diffraction pattern was obtained in the 2θ range of 20–80° considering a fixed counting time and a scan-step of 0.02°. Raman spectra were obtained using the Horiba Jobin Yvon LabRam HR Evolution spectrometer with a 532 nm laser. Scanning electron microscopy (SEM) was performed by using a JEOL JSM-840 Microscope, equipped with an energy-dispersive X-ray spectroscopy (EDS) system (Steroscan 260 EDS analyzer). The micrographs were taken on fracture surfaces. Dielectric measurements have been performed using an HP 4194A Impedance/Gain Phase Analyzer, covering wide frequency and temperature ranges (1 kHz–1 MHz and 50–500 °C, respectively). In order to collect the dielectric parameters, silver paint electrodes were previously applied on both opposite surfaces of the samples.

3. Results and Discussion

Figure 1 shows the XRD patterns obtained at room temperature for the pure BNT sample and BNT–5BT composition. In order to identify the corresponding structural phase and symmetry, as well as to obtain information about the influence of the BT content on the BNT structure, the obtained XRD results were compared to that for the pure BNT system reported in the literature.[23,24] Results revealed that both studied samples have been well-crystallized as perovskite structure, without significant presence of secondary phases. In fact, for the pure BNT sample it has been confirmed the formation of a rhombohedral (R3*c*) FE single phase (ICSD-280983),[23] while for the doped composition (BNT–5BT) it is expected the coexistence of both rhombohedral (R3*c*) FE and tetragonal (P4*bm*) AFE (ICSD-280381) phases.[24]

In order to get more detailed information about the influence of the barium content into the perovskite structure, a magnification in the 2θ region around 32.5–34° has been plotted in the inset of Fig. 2. Result reveals a shift of the reflection peak around 33.2° toward lower angles for the BNT–5BT composition, with respect to the pure BNT sample. This behavior could be related to the difference of the ionic radius (IR) between the Bi^{3+} (~1.40 Å) cation and Ba^{2+} (~1.61 Å) ions at the dodecahedral site of the perovskite structure.[25] Indeed, with the incorporation of the barium cation into the A-site of the perovskite structure, by substituting the bismuth ion, an increase in the volume of the unit-cell is expected, since $IR_{Ba}{}^{2+} > IR_{Bi}{}^{3+}$. Therefore, according to the Bragg's law,[26] a shift of the main peak to a lower 2θ angle, as confirmed by the inset of Fig. 2, reflects an expansion in the unit-cell volume. However, in order to better elucidate these features, additional studies on the structural characteristics, which involves Rietveld structural refinement, should

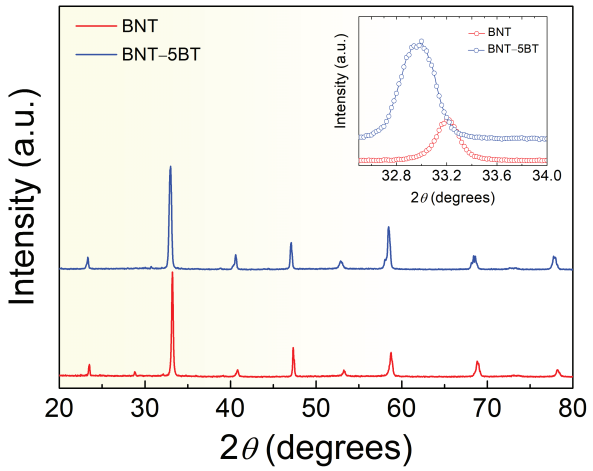

Fig. 2. Room temperature XRD patterns for the studied samples. The inset shows the expanded XRD patterns in the 2θ region around 33.5–34° for both ceramics.

be carried out. Such analyses are in progress and results will be reported in further works.

Figure 3 shows the SEM images and EDS analyses obtained for the studied BNT and BNT–5BT samples ((a) and (b), respectively). It is worth to point out that the micrographs were collected under different magnification scales because of the very high grain size developed for the pure BNT. In this context, even being represented at different scales, results clearly reveal a decrease in the grain-size from around ~15 μm, for the pure BNT sample, up to around 4 μm, for the BNT–5BT composition, noting that the inclusion of the BT content strongly affected the microstructural characteristics. A similar trend in the decrease of the grain size has been reported for other BNT-based compounds,[27,28] and the results have been ascribed to the fact that the doping cations could act as grain growth inhibitors for the hosting BNT system.

Indeed, a possible mechanism for the grain-size reduction in the present study could be associated to the segregation of some A-site cations provided by the doping solution (i.e., Ba^{2+} ions) at the grain boundaries, which act as pinning centers for the effective grain boundary motion during sintering of the samples. As a consequence, this mechanism inhibits the grain growth process. On the other hand, a very low porosity microstructure with uniform and well-defined grains was observed for both compositions, thus confirming the high densification degree in the sintered samples, showing relative densities higher than 90% in both cases. From the technological point of view, highly densified materials with low porosity are very important characteristic for designing high performance electro-electronic components based on lead-free compounds, thus confirming the quality of the studied samples for practical applications. On the other hand, EDS analyses (shown at the bottom of Fig. 3) revealed that both compositions contain the desired elements (Bi, Ba, Na,

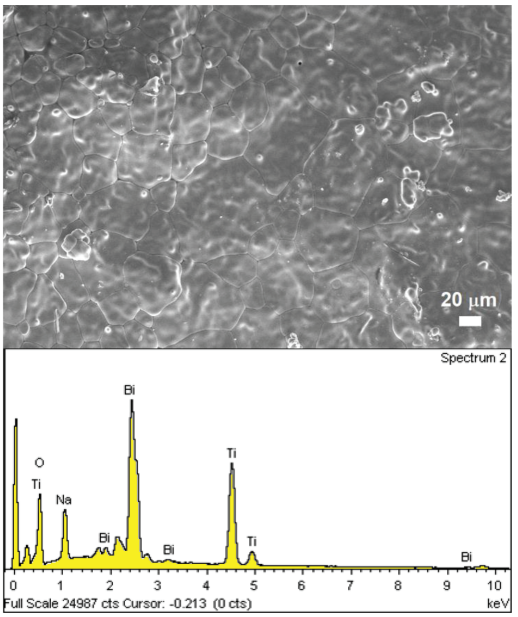

(a)

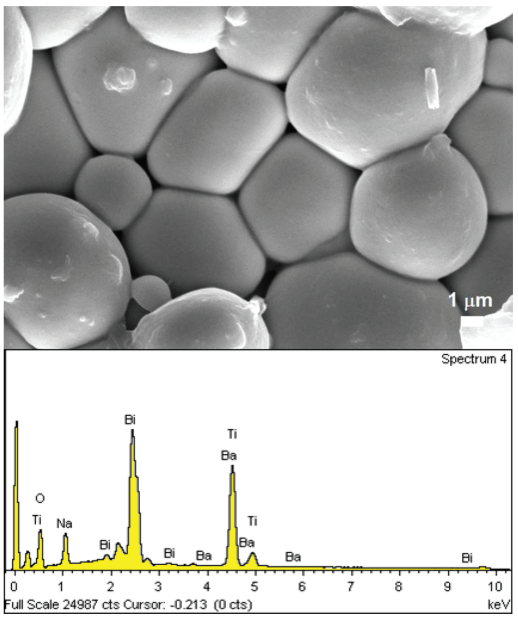

(b)

Fig. 3. SEM images and EDS analyses obtained for the BNT (a) and BNT–5BT (b) samples.

Ti and O) near their surfaces, which confirms the purity of the samples. For both cases (BNT and BNT–5BT samples), A-site (Bi^{3+}, Na^{+}, Ba^{2+}) and B-site (Ti^{4+}) atomic and molecular proportions were close to the expected stoichiometric ratio, confirming that the assumed qualitative compositions were also achieved.

Figure 4 shows the Raman spectra for the studied ceramics and the results reveal similar spectra to those obtained for other BNT-based ceramics.[29,30] The spectra profiles are

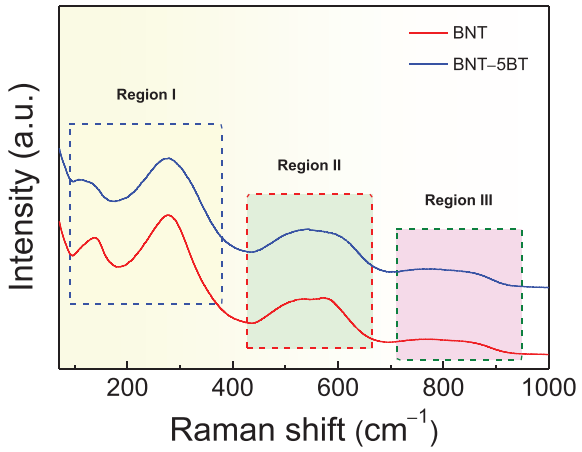

Fig. 4. Room temperature Raman spectra obtained for the studied compositions.

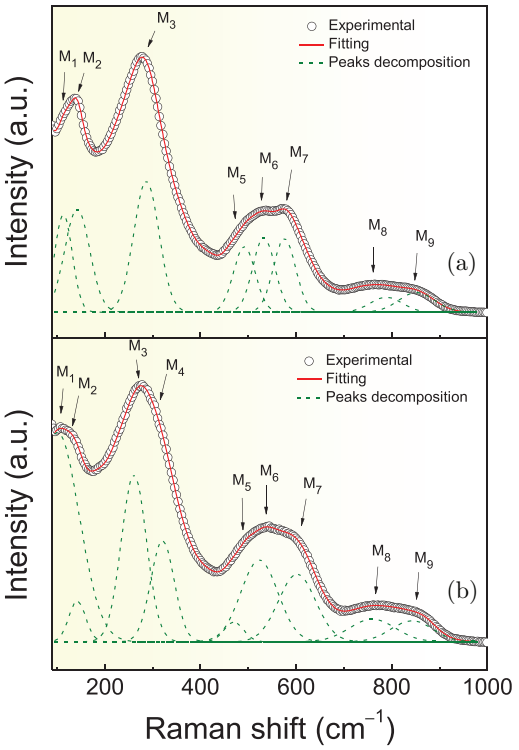

Fig. 5. (Color online) Fitting results (red solid-lines) of the Raman spectra experimental data (open circles) and the decomposed peaks (dark green dashed-lines) for the BNT (a) and BNT–5BT (b) samples.

also characterized by broad Raman bands, which confirm that the perovskite phase was successfully obtained in the studied systems.

The spectra have been divided into three different sections I, II and III, corresponding to the low, middle and high wavenumbers regions, respectively. In order to get additional information on the vibrational modes involved in the three spectral regions, the experimental data shown in Fig. 4 were fitted using a theoretical model reported by Buixaderas *et al.*,[31] which reffers to the location of the curvature maxima in concave-down (CMCD) in spectral region. The fitting results (red solid lines) and the decomposed peaks into Gaussian contributions (dark green dashed lines) are depicted in Fig. 5, where the experimental data are presented as symbols (open circles).

The Raman shift (or wavenumber, cm^{-1}) value, as well as their respective assigned vibrational modes, from M_1 up to M_9, are presented in Table 1 for both samples, where the symmetry assignments have been carried out according to the reported works in the literature for the rhombohedral and tetragonal phases.[32–36] Detailed inspection in the 200–700 cm^{-1} wavenumbers range (regions I and II) reveals additional Raman modes for the BNT–5BT composition, with respect to the pure BNT sample. These extra modes (identified as M_4 and M_7 in Table 1) have been ascribed to a structural change with respect to the pure BNT (with rhombohedral symmetry R3*c*) arisen from the phases coexistence in BNT–BT-based systems.[36,37]

For instance, the coexistence of the ferroelectric (P4*mm*) and AFE (P4*bm*) tetragonal phases has been recently reported for the BNT–*x*BT ceramic system,[38] for compositions where $x = 8$ at.%. Therefore, additional analyses are needed in order to better explore and analyze the influence of the BT content on the BNT unit-cell characteristics. The Raman modes observed in the Regions I and II have been associated to the A–O stretching vibrations in BNT-based compounds,[33] and with the Ti–O stretching vibrations,[36] respectively. The Raman bands observed at higher frequencies (Region III) have been assigned to the stretching modes related to the TiO_6 oxygen octahedra.[39]

For a better investigation about the influence of the BT content on the BNT system, dielectric properties have been also studied and analyzed in a wide temperature and frequency range. Figure 6 shows the temperature dependence of the real

Table 1. Raman shift (RS) and vibrational modes (VM) for the pure (P) and doped (D) samples.

Modes' number	BNT		BNT–5BT	
	RS_P (cm^{-1})	VM_P	RS_D (cm^{-1})	VM_D
M_1	114	$E(TO1)_R$	98	$E(TO1)_R$
M_2	139	$A_1(TO1)_R$	136	$A_1(TO1)_R$
M_3	282	$A_1(TO4)_R$	274	$A_1(TO4)_R$
M_4	—	—	317	$E(LO2)_T$+B1
M_5	496	$A_1(LO7)_R$	496	$A_1(LO7)_R$
M_6	531	$E(TO8)_R$	537	$E(TO8)_R$
M_7	580	$A_1(TO8)_R$	607	$A_1(TO8)_T$
M_8	772	$A_1(LO8)_R$	760	$A_1(LO8)_R$
M_9	858	$A_1(LO9)_R$	861	$A_1(LO9)_R$

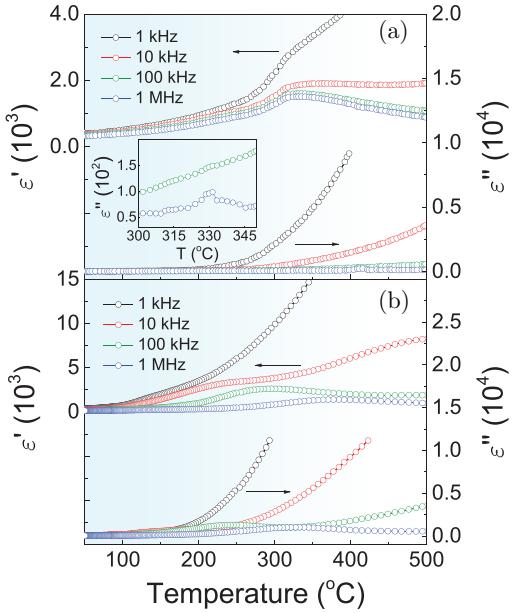

Fig. 6. Temperature dependence of the real (ε') and imaginary (ε'') components of the dielectric permittivity, at different frequencies, for the BNT (a) and BNT–5BT (b) samples.

(ε') and imaginary (ε'') components of the dielectric permittivity, at several frequencies, for the BNT (a) and BNT–5BT (b) samples. Very broad peaks are observed in the dielectric response, over the whole analyzed temperature range, with a strong frequency dispersion for both studied compositions, which indeed seems to be enhanced for the BT-modified sample. This behavior has been associated to the coexistence of different cations (Na^+, Bi^{3+}, Ba^{2+}), showing different valences as well as electronic configuration, in the same dodecahedral crystallographic site of the perovskite structure.[14,40]

It can also be noted that the temperature of the maximum real dielectric permittivity (T_m) decreases with the incorporation of the Ba^{2+} cation into the BNT structure. For instance, at the same frequency, the T_m value reveals to be lower for the BNT–5BT composition than that for the BNT sample, which could be ascribed to the inclusion of the BT content into the BNT perovskite structure. This mechanism seems to promote a coexistence of two crystalline phases (rhombohedral and tetragonal) and confirms the previously discussed results from Raman spectroscopy. An important influence of the electrical conductivity can also be observed in the higher temperature region for both dielectric parameters (ε' and ε''), in particular in the low frequency region. Furthermore, for the BNT–5BT composition, it has also been observed that the temperature for the corresponding maxima of ε' and ε'' (T_m and $T_{m\varepsilon'}$, respectively) appears at different values, which, together with the obtained strong frequency dispersion, could be associated to a relaxor ferroelectric behavior. In this context, the coexistence of different cations (Na^+, Bi^{3+}, Ba^{2+}) at the same crystallographic site leads to a compositional disorder in such a ferroic A-site, thus affecting the long-range polar order. Accordingly, a relaxor-like behavior could be observed. Previous researches have reported that for BT concentrations (x) in the range of 0.06–0.11 a tetragonal (P4*bm* space group) AFE phase, showing a relaxor characteristic in the dielectric response, can coexist with a rhombohedral (R3*c* space group) ferroelectric phase.[41] Therefore, since the BNT–5BT studied composition is very close to the MPB, the observed behaviors in the dielectric response could also be attributed to the coexistence of both rhombohedral and tetragonal phases, thus leading to a possible relaxor-like behavior for the doped sample. It is important to point out that, in order to get more insights on the physical properties of the studied system (pure and modified composition), additional analyses, including ferroelectric response and the relaxation mechanisms that promoted the observed frequency dielectric dispersion, are in progress and results will be presented and better discussed in further works.

4. Conclusion

The structural, microstructural and dielectric properties were investigated in the lead-free pure BNT and BNT–BT solid solution. The obtained results from XRD and Raman spectroscopy revealed well-crystallized ceramics, without significant contribution of secondaries phases. The inclusion of BT on the pure BNT system promoted remarkable structural changes, which can be ascribed to the cationic substitution into the A-site of the perovskite structure. High density ceramics, with well-defined grains and very low porosity offers excellent perspectives for using the BNT–5BT in practical application for electronic devices. Results on the dielectric response revealed a relaxor-like behavior, which could be ascribed to the compositional disorder arisen by the coexistence of different cations (Na^+, Bi^{3+}, Ba^{2+}) at the same crystallographic site, thus affecting the long-range polar order.

Acknowledgments

The authors thank the National Council of Scientific and Technological Development (CNPq) grants 401072/2014-2 and 303447/2019-2, Minas Gerais Research Foundation (FAPEMIG) grants PPM-00661-16 and APQ-02875-18 and Coordenação de Aperfeiçoamento de Pessoal de Nível Superior — Brasil (CAPES) — Finance Code 001 Brazilian agencies for the financial support.

References

[1]M. E. Lines and A. M. Glass, *Principles and Applications of Ferroelectric and Related Material* (Clarendon Press, Oxford, 1977).
[2]Y. Xu, *Ferroelectric Materials and their Applications* (Elsevier Science Publishers, The Netherlands, 1991).
[3]T. Correia and Q. Zhang, *Electrocaloric Materials: New Generation of Coolers* (Springer, Berlin Heidelberg, 2014).

[4]C. Hongbo, Y. Zhenxing, J. Ouyang, Z. Wei and H. Fangren, *Nanostructures in Ferroelectric Films for Energy Applications*, J. Ouyang (ed.), Recent progress in ferroelectric thin film capacitors for high density energy storage (Elsevier Inc., The Netherlands, 2019), pp. 289–308.
[5]K. Uchino K, *Lead-Free Piezoelectrics*, S. Priya and S. Nahm (eds.), Applications of Lead-Free Piezoelectrics (Springer, New York, 2012), pp. 511–528.
[6]RoHS2, Directive 2011/65/EU of the European Parliament and of the European Council on the restriction of the use of certain hazardous substances in electrical and electronic equipment, *Official J. Eur. Union* **L174**, 88 (2011).
[7]Y. Saito, H. Takao, T. Tani, T. Nonoyama, K. Takatori, T. Homma, T. Nagaya and M. Nakamura, Lead-free piezoelectrics, *Nature* **432**, 84 (2004).
[8]S. Zhang and F. Li, High performance ferroelectric relaxor-$PbTiO_3$ single crystals: Status and perspective, *J. Appl. Phys.* **111**, 031301 (2012).
[9]F. Cordero, F. Craciun, F. Trequattrini, E. Mercadelli and C. Galassi, Phase transitions and phase diagram of the ferroelectric perovskite $(Na_{0.5}Bi_{0.5})_{1-x}Ba_xTiO_3$ by anelastic and dielectric measurements, *Phys. Rev. B* **81**, 144124 (2010).
[10]I. Coondoo, N. Panwar and A. Kholkin, Lead-free piezoelectrics: Current status and perspectives, *J. Adv. Dielectr.* **3**, 1330002 (2013).
[11]H. Du, W. Zhou, F. Luo, D. Zhu, S. Qu, Ye Li and Z. Pei, Design and electrical properties investigation of $(K_{0.5}Na_{0.5})NbO_3$–$BiMeO_3$ lead-free piezoelectric ceramics, *J. Appl. Phys.* **104**, 034104 (2008).
[12]P. K. Panda, Review: Environmental friendly lead-free piezoelectric materials, *J. Mater. Sci.* **44**, 5049 (2009).
[13]E. Aksel and J. L. Jones, Advances in lead-free piezoelectric materials for sensors and actuators, *Sensors* **10**, 1935 (2010).
[14]C. Xu, D. Lin and K.W. Kwok, Structure, electrical properties and depolarization temperature of $(Bi_{0.5}Na_{0.5})TiO_3$–$BaTiO_3$ lead-free piezoelectric ceramics, *Solid State Sci.* **10**, 934 (2008).
[15]Y. Guo, Y. Liu, R. L. Withers, F. Brink and H. Chen, Large electric field-induced strain and antiferroelectric behavior in $(1–x)$-$(Na_{0.5}Bi_{0.5})TiO_{3–x}BaTiO_3$ ceramics, *Chem. Mater.* **23**, 219 (2011).
[16]R. R. McQuade and M. R. Dolgos, A review of the structure-property relationships in lead-free piezoelectric $(1–x)$-$Na_{0.5}Bi_{0.5}TiO_3$–$(x)BaTiO_3$, *J. Solid State Chem.* **242**, 140 (2016).
[17]T. Takenaka, K. Maruyama and K. Sakata, $(Bi_{1/2}Na_{1/2})TiO_3$-$BaTiO_3$ system for lead-free piezoelectric ceramics, *Jpn. J. Appl. Phys.* **30**, 2236 (1991).
[18]C. Ma and X. Tan, Phase diagram of unpoled lead-free $(1–x)$-$(Bi_{1/2}Na_{1/2})TiO_{3–x}BaTiO_3$ ceramics, *Solid State Commun.* **150**, 1497 (2010).
[19]T. R. Shrout and S. J. Zhang, Lead-free piezoelectric ceramics: Alternatives for PZT? *J. Electroceram.* **19**, 113 (2007).
[20]J. Shi, H. Fan and Z. Li, Electromechanical properties and microstructure evolution of BNT–BT piezoelectric ceramics, *Ferroelectrics* **404**, 93 (2010).
[21]T. Badapanda, S. Sahoo and P. Nayak, Dielectric, ferroelectric and piezoelectric study of BNT-BT solid solutions around the MPB region, *IOP Conf. Ser.: Mater. Sci. Eng.* **178**, 012032 (2017).
[22]W. D. Kingery, H. K. Bowen and D. R. Uhlmann, *Introduction to Ceramics* (John Wiley & Sons, New York, 1976).
[23]G. O. Jones and P. A. Thomas, Investigation of the structure and phase transitions in the novel A-site substituted distorted perovskite compound $Na_{0.5}Bi_{0.5}TiO_3$, *Acta Cryst. B* **58**, 168 (2002).
[24]G. O. Jones and P. A. Thomas, The tetragonal phase of $Na_{0.5}Bi_{0.5}TiO_3$ — A new variant of the perovskite structure, *Acta Cryst. B* **56**, 426 (2000).
[25]R. D. Shannon, Revised effective ionic radii and systematic studies of interatomic distances in halides and chalcogenides, *Acta Cryst. A* **32**, 751 (1976).
[26]B. D. Cullity, *Elements of X-Ray Diffraction* (Addison-Wesley Publishing Company, Inc., London, 1967).
[27]M. Zannen, A. Lahmar, M. Dietze, H. Khemakhem, A. Kabadou and M. Es-Souni, Structural, optical, and electrical properties of Nd-doped $Na_{0.5}Bi_{0.5}TiO_3$, *Mater. Chem. Phys.* **134**, 829 (2012).
[28]Z.-H. Zhao, R.-F. Ge and Y. Dai, Large electro-strain signal of the BNT–BT–KNN lead-free piezoelectric ceramics with CuO doping, *J. Adv. Dielectr.* **9**, 1950022 (2019).
[29]J. Suchanicz, I. Jankowska-Sumara and T. V. Kruzina, Raman and infrared spectroscopy of $Na_{0.5}Bi_{0.5}TiO_3$-$BaTiO_3$ ceramics, *J. Electroceram.* **27**, 45 (2011).
[30]R. Garg, B. N. Rao, A. Senyshyn, P. S. R. Krishna and R. Ranjan, Lead-free piezoelectric system $(Na_{0.5}Bi_{0.5})TiO_3$-$BaTiO_3$: Equilibrium structures and irreversible structural transformations driven by electric field and mechanical impact, *Phys. Rev. B* **88**, 014103 (2013).
[31]E. Buixaderas, V. Bovtun, M. Kempa, D. Nuzhnyy, M. Savinov, P. Vanek, I. Gregora and B. Malic, Lattice dynamics and domain wall oscillations of morphotropic Pb(Zr, Ti)O_3 ceramics, *Phys. Rev. B* **94**, 054315 (2016).
[32]U. D. Venkateswaran, V. M. Naik and R. Naik, High-pressure Raman studies of polycrystalline $BaTiO_3$, *Phys. Rev. B* **58**, 14256 (1998).
[33]J. Kreisel, A. M. Glazer, G. Jones, P. A. Thomas, L. Abello and G. Lucazeau, An X-ray diffraction and Raman spectroscopy investigation of A-site substituted perovskite compounds: The $(Na_{1-x}K_x)_{0.5}Bi_{0.5}TiO_3$ $(0 \le x \le 1)$ solid solution, *J. Phys.: Condens. Matter* **12**, 3267 (2000).
[34]P. S. Dobal, A. Dixit, R. S. Katiyar, Z. Yu, R. Guo and A. S. Bhalla, Micro-Raman scattering and dielectric investigations of phase transition behavior in the $BaTiO_3$–$BaZrO_3$, *J. Appl. Phys.* **89**, 8085 (2001).
[35]M. K. Niranjan, T. Karthik, S. Asthana, J. Pan and U. V. Waghmare, Theoretical and experimental investigation of Raman modes, ferroelectric and dielectric properties of relaxor $Na_{0.5}Bi_{0.5}TiO_3$, *J. Appl. Phys.* **113**, 194106 (2013).
[36]V. Pal, O. P. Thakur and R. K. Dwivedi, Investigation of MPB region in lead free BLNT-BCT system through XRD and Raman spectroscopy, *J. Phys. D: Appl. Phys.* **48**, 055301 (2015).
[37]C. M. Lau, X. Wu and K. W. Kwok, Effects of vacancies on luminescence of Er-doped $0.93Bi_{0.5}Na_{0.5}TiO_3$–$0.07BaTiO_3$ ceramics, *J. Appl. Phys.* **118**, 034107 (2015).
[38]Y. Mendez-González, A. Peláiz-Barranco, J. D. S. Guerra, A. Pentón-Madrigal and P. Saint-Grégoire, Effect of the lanthanum concentration on the physical properties of the $(Bi_{0.5}Na_{0.5})_{0.92}Ba_{0.08\text{-}3x/2}La_xTiO_3$ ceramic system, *Mater. Chem. Phys.* **208**, 103 (2018).
[39]J. Shi, H. Fan, X. Liu and A. J. Bell, Large Electrostrictive strain in $(Bi_{0.5}Na_{0.5})TiO_3$–$BaTiO_3$–$(Sr_{0.7}Bi_{0.2})TiO_3$ solid solutions, *J. Am. Ceram. Soc.* **97**, 848 (2014).
[40]M. Zhu, L. Liu, Y. Hou, H. Wang and H. Yan, Microstructure and electrical properties of MnO–doped $(Na_{0.5}Bi_{0.5})_{0.92}Ba_{0.08}TiO_3$ lead-free piezoceramics, *J. Am. Ceram. Soc.* **90**, 120 (2007).
[41]C. Ma, X. Tan, E. Dul'kin and M. Roth, Domain structure-dielectric property relationship in lead-free $(1–x)Bi_{1/2}Na_{1/2}TiO_{3–x}BaTiO_3$ ceramics, *J. Appl. Phys.* **108**, 104105 (2010).